Structure of GeO_2 glass at pressures up to 8.6 GPa

James W. E. Drewitt,[1] Philip S. Salmon,[1] Adrian C. Barnes,[2] Stefan Klotz,[3] Henry E. Fischer,[4] and Wilson A. Crichton[5,6]
[1]*Department of Physics, University of Bath, Bath BA2 7AY, United Kingdom*
[2]*H. H. Wills Physics Laboratory, Royal Fort, Tyndall Avenue, Bristol BS8 1TL, United Kingdom*
[3]*IMPMC, Université Pierre et Marie Curie, F-75252 Paris, France*
[4]*Institut Laue-Langevin, 6 rue Jules Horowitz, BP 156, Grenoble Cedex 9 F-38042, France*
[5]*European Synchrotron Radiation Facility, 6 rue Jules Horowitz, BP 220, Grenoble Cedex F-38043, France*
[6]*Department of Earth Sciences, University College London, Gower Street, London WC1E 6BT, United Kingdom*
(Received 30 August 2009; revised manuscript received 4 November 2009; published 11 January 2010)

The structure of GeO_2 glass at pressures extending from ambient to 8.6(5) GPa was measured at $\simeq$25 °C by using *in situ* neutron diffraction. The results show a gradual change in the intermediate range order with increasing density as manifested by an increase in position and reduction in height of the first sharp diffraction peak in the total structure factor. By contrast, the local ordering, as characterized by the Ge-O bond length and coordination number, remains constant for the pressure range from ambient to $\simeq$5 GPa. As the pressure is increased further to 8.6(5) GPa, however, a steady increase from 4.0(1) to 4.9(1) is observed in the Ge-O coordination number as the corresponding distance increases from 1.73(2) to 1.77(2) Å. The results are therefore consistent with the operation of two densification mechanisms, the low-pressure one associated with squeezing the open network of corner-linked tetrahedral motifs and the high-pressure one associated with a transformation of those motifs. There is no evidence in support of an abrupt transformation of the network structure over the investigated pressure range. The structure of permanently densified GeO_2 glass was also investigated by high-energy x-ray diffraction. The results show that there is a threshold pressure at $\simeq$5 GPa below which the structure of a recovered glass is similar to that of the high-pressure material. Above the threshold pressure there is, however, a reorganization of both the local and intermediate range ordering once the pressure is released and the Ge-O coordination number returns to 4.

DOI: 10.1103/PhysRevB.81.014202 PACS number(s): 61.43.Fs, 61.05.fm, 62.50.−p, 64.70.kj

I. INTRODUCTION

Germania, or GeO_2, is a classic example of a "strong" network glass forming system[1] which shares with silica several structural characteristics,[2,3] including a transformation of the glass from a network of corner-sharing tetrahedra under ambient conditions to a dense octahedral material at high pressure.[4–12] The transformations do, however, occur at much lower pressures in the case of GeO_2 which makes them more amenable to study by using different experimental methods.[6,10,13] In addition, the neutron and x-ray scattering lengths are greater in the case of Ge compared to Si, which is beneficial when employing the small samples required for high-pressure diffraction experiments. The coherent neutron-scattering length contrast for the isotopes of Ge is also larger than for Si, which means that it may be feasible to extract the full set of partial structure factors under pressure by using the method of isotope substitution in neutron diffraction.[14–16]

In order to investigate the nature of the pressure-induced structural transformations in glassy GeO_2, and hence provide insight into the accompanying changes in the physical properties of this material, it is necessary to conduct *in situ* high-pressure experiments. For example, samples that have been pressurized and then recovered to ambient conditions show no change in the Ge-O coordination number from its ambient value of 4, which indicates recovery of the local order, although the intermediate range order is permanently altered.[5,7,17,18] The purpose of the present paper is to report results on the structure of vitreous GeO_2 under pressure which demonstrate *inter alia* the recent development of neutron-diffraction methods to accurately measure the structure of glassy materials *in situ* at pressures extending to $\simeq$8.5 GPa. In particular, the nature of the structural transformation of GeO_2 glass from an open network of corner-shared GeO_4 tetrahedra to a dense network of polyhedra with a mean Ge-O coordination number of 5 is investigated. Outstanding issues include the sharpness of the transition[19–21] and the existence, or otherwise, of GeO_5 units in addition to the GeO_4 and GeO_6 units found in the α-quartzlike and rutile forms of crystalline GeO_2.[10] There is also the question about the extent to which a competition between ordering on the intermediate and extended length scales provides a means for rationalizing the density-dependent transitions that occur in tetrahedral network glass forming systems.[14,22–24] The experiments were made by mounting a Paris-Edinburgh (PE) press on the neutron diffractometer D4C (Ref. 25) at the reactor source of the Institut Laue-Langevin, Grenoble. The structure of as-prepared uncompressed GeO_2 glass and the material recovered from a neutron-diffraction experiment at 8.0(5) GPa was also studied by using high-energy x-ray diffraction at the European Synchrotron Radiation Facility (ESRF), Grenoble.

The paper is organized as follows. In Sec. II the essential theory is given and in Sec. III the experimental procedure is described. The data-reduction method for the *in situ* high-pressure neutron-diffraction experiments is then outlined in Sec. IV. The results are presented in Sec. V and are discussed in Sec. VI by reference to several of the results previously obtained on the pressure-induced transformations in germania from diffraction[9,14,15,17,18,21,26–29] and spectroscopic[5–7,12,13,21,30–35] methods. The results from sev-

eral molecular-dynamics studies of germania, using effective interatomic potentials[36–50] or first-principles methods,[48,50–52] are also considered. Concluding remarks are given in Sec. VII.

II. THEORY

In a neutron-diffraction experiment on glassy GeO_2 the scattered intensity containing structural information can be represented by the total structure factor[53]

$$F_N(k) = \sum_{\alpha=1}^{n} \sum_{\beta=1}^{n} c_\alpha c_\beta b_\alpha b_\beta [S_{\alpha\beta}(k) - 1], \quad (1)$$

where α and β denote the chemical species, $n=2$ is the number of different chemical species, c_α and b_α represent the atomic fraction and bound coherent scattering length of chemical species α, $S_{\alpha\beta}(k)$ is a Faber-Ziman[54] partial structure factor, and k is the scattering vector. The coherent neutron-scattering lengths for Ge and O are 8.185(20) and 5.803(4) fm, respectively.[55] $S_{\alpha\beta}(k)$ is related to the partial pair-distribution function $g_{\alpha\beta}(r)$ by the Fourier-transform relation

$$g_{\alpha\beta}(r) - 1 = \frac{1}{2\pi^2 n_0 r} \int_0^\infty dk k [S_{\alpha\beta}(k) - 1] \sin(kr), \quad (2)$$

where n_0 is the atomic number density and r is a distance in real space. The mean coordination number of atoms of type β, contained in a volume defined by two concentric spheres of radii r_i and r_j centered on an atom of type α, is given by

$$\bar{n}_\alpha^\beta = 4\pi n_0 c_\beta \int_{r_i}^{r_j} dr r^2 g_{\alpha\beta}(r). \quad (3)$$

Often the total structure factor is rewritten as

$$S_N(k) = F_N(k)/\langle b \rangle^2 + 1, \quad (4)$$

where $\langle b \rangle = c_{Ge} b_{Ge} + c_O b_O$ is the mean coherent scattering length. The corresponding real-space information is provided by the total pair-distribution function $G_N(r)$ which is obtained from the Fourier transform relation

$$G_N(r) - 1 = \frac{1}{2\pi^2 n_0 r} \int_0^\infty dk k [S_N(k) - 1] \sin(kr). \quad (5)$$

For r values smaller than the distance of closest approach between the center of two atoms $g_{\alpha\beta}(r) = g_{\alpha\beta}(r=0) = 0$ such that $G_N(r) = G_N(r=0) = 0$.

In an x-ray diffraction experiment on GeO_2 glass Eqs. (1), (4), and (5) remain valid provided that each b_α is replaced by the corresponding k-dependent x-ray form factor $f_\alpha(k)$ such that Eq. (4) becomes $S_X(k) = F_X(k)/|\langle f(k) \rangle|^2 + 1$, where the average x-ray form factor $\langle f(k) \rangle = c_{Ge} f_{Ge}(k) + c_O f_O(k)$.[53]

III. EXPERIMENTAL

A. Sample preparation

Two batches of glass of mass ≈ 3 g were made from GeO_2 powder (99.9999%, Alfa Aesar). The first batch was made by heating the powder in a Pt-10% Rh crucible in air at 1600 °C for $\simeq 30$ min before placing the crucible on a liquid-nitrogen-cooled brass block and dousing with liquid nitrogen. The sample was subsequently annealed near the glass transition temperature T_g for $\approx$ 30 min to remove residual stress as for optical experiments.[56–58] The second batch was made by using the procedure described elsewhere and did not incorporate this annealing process.[15] The thermal characteristics of the glass from the first batch were measured by modulated differential scanning calorimetry using a TA Instruments DSC Q100 machine with a finned air cooling system. The glassy samples were held in pans made from 0.025-mm-thick gold foil (99.99%, Aldrich) which had been annealed at 750 °C for 3 h to remove residual stress. The measurements were made using a scan rate of 3 °C min^{-1} with a temperature modulation of ± 0.5 °C per 100 s under an oxygen-free nitrogen gas flow. The reversible heat-flow signal gave T_g (midpoint) = 566(2) °C which compares with previously reported values of 476(7) °C (Ref. 59), 545 °C (Ref. 60), 550 °C (Refs. 61 and 62), and 578–584 °C (Ref. 63).

B. Neutron-diffraction experiments

Two separate neutron-diffraction experiments on glassy GeO_2 at high pressure and ambient temperature ($\simeq 25$ °C) were made by mounting a VX5/180-type PE press, with two support pillars and standard sintered cubic boron nitride (BN) single toroid anvils,[64,65] on the diffractometer D4C (Ref. 25) at the Institut Laue-Langevin. The first batch of glass was used in study A with an incident neutron wavelength of 0.6957(1) Å while the second batch of glass was used in study B with an incident neutron wavelength of 0.6960(1) Å. This choice of wavelength maximizes the incident flux of neutrons. The background scattering was reduced by covering the anvils with neutron absorbing Cd metal and by using neutron absorbing $^{10}B_4C$ slits placed a few cm upstream of the sample to reduce the vertical divergence of the incident beam. The most notable difference between studies A and B was the use of improved neutron shielding in the second experiment to reduce the scattered intensity from the Paris-Edinburgh press. Each sample was in the form of a pellet made from finely powdered glass which had been precompacted to the correct geometry. The sample was held in a single toroid gasket made from a null scattering Ti-Zr alloy with a mean coherent neutron-scattering length of zero. The gasket and collimation provided by the neutron absorbing BN anvils defined a cylindrical sample geometry with the incident and scattered beams in a plane perpendicular to the axis of the cylinder, i.e., both beams passed through the gasket material. The sample diameter and height under ambient conditions were 6 and 1.6 mm, respectively.

For each study, diffraction patterns were measured for the sample contained in a gasket with a small applied load (corresponding to an oil pressure of ≤ 100 bars applied to a piston of area 66.5 cm^2) to ensure that the gasket material took the shape of the anvils (effectively ambient pressure) and at several pressure points up to 8.6(5) GPa. To estimate the

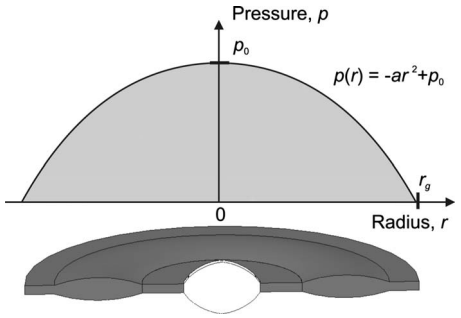

FIG. 1. A schematic showing the parabolic pressure profile assumed for the sample and gasket assembly in the Paris-Edinburgh press (upper illustration) compared to a section through the compressed assembly with the sample position located centrally (lower illustration).

container scattering, diffraction patterns were measured for an empty uncompressed (i.e., unsquashed) Ti-Zr gasket and also for empty Ti-Zr gaskets that had been recovered from different high pressures. To assist in the data normalization at different pressures, diffraction patterns were measured for two differently sized vanadium pellets in an unsquashed or recovered (i.e., presquashed) Ti-Zr gasket at ambient pressure. In addition, a diffraction pattern was measured for the empty anvils (corresponding to an anvil spacing of ≥ 0.4 mm) to assist in estimating the background scattering and, to examine the effect of sample self-shielding on the background count rate at small scattering angles,[66] diffraction patterns were measured for two differently sized neutron absorbing Cd pellets in an unsquashed or recovered Ti-Zr gasket at ambient pressure. The sample self-shielding correction using Cd was found to be small and, in practice, the correction was not made.

The sample pressure was determined from the load L applied to the anvils by using a calibration based on many neutron-diffraction experiments using crystalline systems with a known equation of state in an otherwise identical setup.[67] Specifically, a parabolic profile was assumed for the pressure $p(r)$ on the sample and gasket assembly at a distance r from the center of symmetry (see Fig. 1) such that $p(r)=-ar^2+p_0$, where p_0 is the maximum pressure at the sample position. The boundary conditions are $p(r=0)=p_0$ and $p(r_g)=0$, where r_g is the outer radius of the gasket, so that the constant $a=p_0/r_g^2$. The total force applied to the sample and gasket assembly is given by $F(r_g)=Lg=2\pi\int_0^{r_g} drrp(r)=\pi p_0 r_g^2/2$, where g is the acceleration due to gravity. This equation can be rearranged to give

$$p_0 = 2F(r_g)/A = (2g/\pi r_g^2)L, \tag{6}$$

where $A=\pi r_g^2$ is the area of the sample and gasket assembly. Figure 2 compares the calibration curve thus produced with the results obtained separately from a variety of crystalline samples. The new data points were obtained from the r_g values measured for Ti-Zr gaskets recovered from high-pressure neutron-diffraction experiments on GeO_2 glass (studies A and B of the present work) and GeS_2 glass.[68] The calibration curve assumes a linear relation between the pressure and load after application of an initial load of

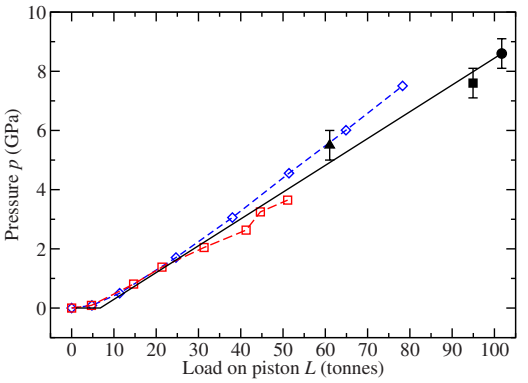

FIG. 2. (Color online) Load L applied to the piston of the VX5 variant Paris-Edinburgh press versus the pressure p at the sample position from measurement of the diffraction pattern for various powdered samples at 300 K (Ref. 67) [(blue) ◇] and LiCl doped ice with a small amount of lead at 85 K (Ref. 67) [(red) □]. The pressure was also obtained from Eq. (6) by using the measured outer radius of the Ti-Zr gasket recovered from high-pressure diffraction experiments on GeO_2 glass in studies A (●) and B (■) of the present work and on GeS_2 glass (Ref. 68) (▲). The calibration curve [solid (black) curve] was obtained by assuming that no pressure is applied to the sample for $0 \leq L$ (tonne) $\lesssim 7$, as the gasket material initially takes the shape of the anvils, and that a linear relation holds for higher loads.

$\gtrsim 7$ tonne; for small initial loads the gasket deforms to the shape of the anvils but negligible pressure is applied to the sample. The validity of this pressure determination has been verified by many experiments on powdered crystalline samples carried out over the last 15 years using exactly the same gasket and anvil geometry (S. Klotz, private communication). The pressure values thus deduced are accurate to better than $\pm 10\%$.

In Fig. 3 the pressure dependence of the density of GeO_2 glass, obtained from the *in situ* measurements of Hong *et al.*,[21,69] Smith *et al.*,[70] and Tsiok *et al.*,[71] is compared with the results obtained by Sharma *et al.*[30] for glasses formed by quenching the liquid at different pressures. The densities used in the neutron-diffraction data analysis (see Table I) were obtained from the results of Hong *et al.*[21] which are in good agreement with those of Tsiok *et al.*[71] The densities measured for GeO_2 glass recovered from high pressure to ambient conditions are also illustrated in Fig. 3.[17,18,34,72,73] The data point from Ref. 73 is assumed to correspond to the highest pressure attained in Ref. 72. The *in situ* and recovered sample densities are comparable for pressures up to ≈ 4 GPa. However, at higher pressures the density of the recovered samples is significantly smaller.

The equation of state for the null scattering Ti-Zr alloy used for the gasket material has not been measured although it has been investigated in the case of elemental Ti (Refs. 74 and 75) and Zr (Refs. 76–80) and in the case of the equiatomic alloy TiZr.[81,82] Titanium forms a hexagonal-close-packed α phase under ambient conditions which transforms at ambient temperature to a hexagonal ω phase at 7.4–9 GPa.[74,75] Zirconium and the equiatomic alloy show similar behavior, the α-to ω-phase transformation taking place at 5.5–6.7 GPa for Zr (Refs. 77, 78, and 80) and

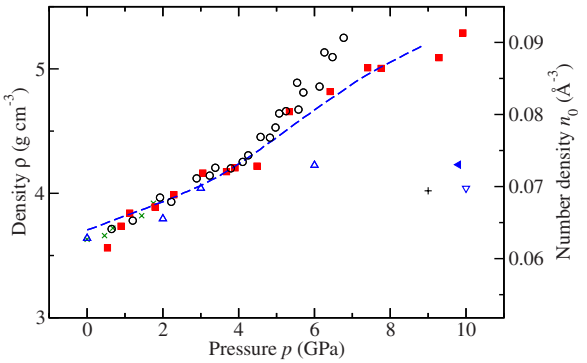

FIG. 3. (Color online) The mass density ρ and corresponding number density n_0 for GeO_2 glass as measured on compression in the *in situ* studies of Hong *et al.* (Ref. 21) [(red) ■], Smith *et al.* (Ref. 70) (○), and Tsiok *et al.* (Ref. 71) [broken (blue) curve]. The values obtained by Sharma *et al.* (Ref. 30) [(green) ×] for glasses formed by quenching the liquid at different pressures are also shown. The data sets are compared with the values measured for samples recovered from high pressure to ambient conditions by Stone *et al.* (Ref. 17) [(blue) △], Ishihara *et al.* (Ref. 34) (+), Sampath *et al.* (Ref. 18) [(blue) ▽], and Cohen and Roy (Refs. 72 and 73) [(blue) ◀].

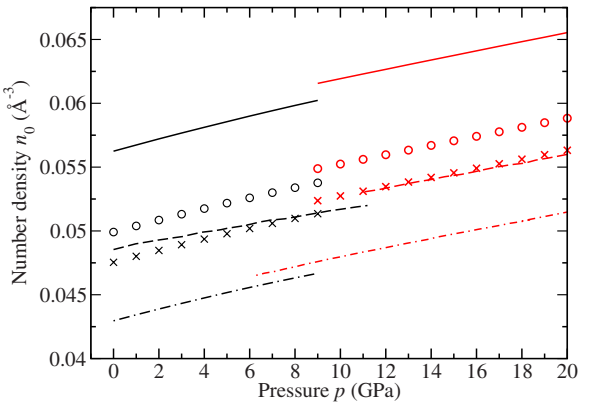

FIG. 4. (Color online) The number density n_0 as a function of pressure p at room temperature as measured for Ti (Ref. 74) (solid curves), Zr (Ref. 80) (chained curves), and the equiatomic alloy TiZr (Ref. 81) (broken curves). The dark (black) curves at low pressures correspond to the α phases and the light (red) curves at high pressures correspond to the ω phases of these materials. The curve for α-Zr shown in the range $\approx$6–9 GPa is an extrapolation. Also shown is the number density for the equiatomic alloy TiZr (×) and the null scattering alloy $Ti_{0.676}Zr_{0.324}$ (○) as calculated by using Vegard's law.

11.0 ± 1.5 GPa for TiZr.[81] According to Vegard's law the number density of the alloy can be deduced from a linear combination of the number densities of the individual components, e.g., $n_0(\alpha\text{-TiZr}) = c_{Ti} n_0(\alpha\text{-Ti}) + c_{Zr} n_0(\alpha\text{-Zr})$. The data for α-Zr (Ref. 80) were extrapolated to 9 GPa and, as shown in Fig. 4, an application of Vegard's law reproduces the measured density of α-TiZr to within 2%. The measured density of ω-TiZr is also compared with the prediction of Vegard's law in Fig. 4. The coherent neutron-scattering lengths of Ti and Zr are −3.438(2) and 7.16(3) fm, respectively,[55] which gives $Ti_{0.676}Zr_{0.324}$ as the null scattering composition. Vegard's law was also used to find the density of this null scattering Ti-Zr alloy, assuming that this material also forms distinct α and ω phases (see Fig. 4). At ambient pressure the value $n_0 = 0.0511(5)$ Å^{-3} was measured for $Ti_{0.676}Zr_{0.324}$ by weighing the material in fluids (water and air) of different density and applying Archimedes' principle. Vegard's law reproduces this value to within 2%.

In the case of the gasket a force $F_g = F(r_g) - F(r_g')$ is applied by the anvils to an annular surface of area $A_g = \pi(r_g^2 - r_g'^2)$, where r_g' is the inner radius of the gasket. The average pressure exerted across the gasket is therefore given by

TABLE I. Several of the parameters describing the pressure dependence of the structure of GeO_2 glass as obtained from neutron-diffraction studies A and B. The number density n_0 of the glass is given together with the position k_{FSDP} of the first sharp diffraction peak, the position k_{PP} of the principal peak, the Ge-O bond distance r_{GeO}, the corresponding mean coordination number $\bar{n}_{Ge}^{O}$, and the second peak position r_2 in $G_N(r)$.

p (GPa)	n_0 (Å^{-3})	k_{FSDP} (Å^{-1})	k_{PP} (Å^{-1})	r_{GeO} (Å)	$\bar{n}_{Ge}^{O}$	r_2 (Å)	Study
Ambient	0.0629(3)	1.55(2)	2.65(2)	1.73(2)	3.9(1)	2.85(3)	A
Ambient	0.0629(3)	1.53(2)	2.68(3)	1.74(2)	4.0(1)	2.78(3)	B
1.2(5)	0.0664(9)	1.52(2)	2.67(2)	1.73(2)	4.0(1)	2.98(3)	A
2.2(5)	0.0684(9)	1.60(2)	2.65(3)	1.73(2)	4.0(1)	2.84(3)	B
3.1(5)	0.0719(9)	1.62(2)	2.74(2)	1.73(2)	4.1(1)	3.01(3)	A
4.0(5)	0.0726(9)	1.71(2)	2.71(2)	1.73(2)	4.0(1)	2.84(3)	B
4.9(5)	0.0774(9)	1.81(2)	2.72(2)	1.74(2)	4.1(1)	2.85(3)	A
4.9(5)	0.0774(9)	1.80(2)	2.73(2)	1.73(2)	4.1(1)	3.00(3)	B
5.8(5)	0.0816(9)	1.82(2)	2.72(2)	1.74(2)	4.2(1)	2.79(3)	B
6.8(5)	0.0845(9)	1.92(2)	2.78(2)	1.75(2)	4.6(1)	2.94(3)	A
8.0(5)	0.0866(9)	1.96(2)	2.81(2)	1.75(2)	4.4(1)	2.79(3)	B
8.6(5)	0.0872(9)	2.09(5)	2.77(5)	1.77(2)	4.9(1)	2.90(3)	A

$$p_g = \frac{F_g}{A_g} = \frac{p_0 r_g^2}{(r_g^2 - r_g'^2)} \left\{ \frac{1}{2} - \left(\frac{r_g'}{r_g} \right)^2 + \frac{1}{2} \left(\frac{r_g'}{r_g} \right)^4 \right\}. \quad (7)$$

Equation (7) and the data in Fig. 4 were used to estimate the density of the Ti-Zr gasket at each pressure point for use in the data analysis. The values of r_g and r_g' for each pressure point were estimated from the measured values for uncompressed and recovered gaskets.

C. High-energy x-ray diffraction experiments

A high-energy x-ray diffraction experiment was made on the GeO_2 glass sample recovered from 8.0(5) GPa a few hours after the end of neutron-diffraction study B. A piece of the as-prepared glass was also investigated at the same time. The x-ray diffraction experiments were made using beamline ID11 at the ESRF with an incident x-ray wavelength of 0.1220 Å and a FReLoN 2k16 charge-coupled device (CCD) detector with a 200-μm-thick P43 phosphor and detection field of 94×94 mm^2 with a pixel size of 48×48 μm^2.[83] Two-dimensional diffraction patterns were taken for the samples and instrument background at two sample to detector distances of 160 and 300 mm with an acquisition time of 20 s per pattern. The centering of the diffraction image on the CCD and the wave-vector k calibration were found by measuring the powder-diffraction patterns for a crystalline silicon standard. The diffraction images for the samples were reduced to one-dimensional patterns by using the program FIT2D.[84] These patterns were then corrected for background scattering and normalized by fitting to the sum of the self-scattering and Compton[85] scattering contributions to the x-ray differential scattering cross section at high-k values.[53] Neutral atom form factors were used for Ge and O.[86]

IV. HIGH-PRESSURE NEUTRON-DIFFRACTION DATA REDUCTION

The neutron-diffraction data-analysis procedure is not straightforward as the scattering geometry changes with pressure (e.g., the sample compresses as the anvils close) and it is not possible to make all of the necessary measurements for the data reduction at each pressure point. In a conventional neutron-diffraction experiment using reactor-based instrumentation the total structure factor $F_N(k)$ is extracted from the measured intensities by using the relations[87]

$$\frac{d\sigma}{d\Omega} \equiv F_N(k) + \sum_{\alpha=1}^{n} c_\alpha [b_\alpha^2 + b_{\mathrm{inc},\alpha}^2][1 + P_\alpha(k)]$$
$$= \frac{1}{N_s A_{s,sc}(\theta)} \left\{ \left[\frac{I_{sc}(\theta)}{a(\theta)} - M_{sc}(\theta) \right] - \frac{A_{c,sc}(\theta)}{A_{c,c}(\theta)} \left[\frac{I_c(\theta)}{a(\theta)} - M_c(\theta) \right] \right\}, \quad (8)$$

where $d\sigma/d\Omega$ represents the measured differential scattering cross section, $k=(4\pi/\lambda)\sin\theta$, λ is the incident neutron wavelength, 2θ is the scattering angle, and $a(\theta)$ is a normalization factor measured by reference to a vanadium standard.[88] In Eq. (8), $b_{\mathrm{inc},\alpha}$ represents the bound incoherent-scattering length of chemical species α, N_s is the number of sample atoms illuminated by the incident beam, and the $P_\alpha(k)$ terms arise from inelasticity effects which are often calculated in terms of the moments of the dynamical structure factor.[89] The attenuation factors $A_{i,j}(\theta)$ refer to neutrons that are scattered in medium i and attenuated, through absorption and scattering, in medium j (Ref. 90) and the multiple-scattering cross sections $M_i(\theta)$ can be calculated in the quasi-isotropic approximation.[91] The quantities $I_{sc}(\theta) \equiv I_{sc}^E(\theta) - I_b^E(\theta)$ and $I_c(\theta) \equiv I_c^E(\theta) - I_b^E(\theta)$ represent the measured intensities $I_{sc}^E(\theta)$ and $I_c^E(\theta)$ for the sample (s) in its container (c) and for the empty container, respectively, corrected for background scattering $I_b^E(\theta)$. At small 2θ values the correction for background scattering $I_b^E(\theta)$ is often modified by reference to a Cd absorber in order to take into account the effect of sample self-shielding on the background count rate.[66]

In the case of high-pressure experiments it is difficult to measure exactly the contribution to the scattering from the gasket and background at each pressure point. For instance, an empty gasket in the press under a given applied load will not replicate a gasket under the same load with the sample present because the mechanical properties of the sample will affect the gasket deformation. It is therefore necessary to estimate the contribution from the gasket and background at each pressure point by the use of a suitable interpolation procedure. For example, if the intensities are measured for an uncompressed gasket $I_c^E(\theta)$, recovered gasket $I_{c'}^E(\theta)$, and empty anvils $I_b^E(\theta)$ then the first-order correction is to assume a linear combination of the background-corrected empty gasket intensities such that Eq. (8) is rewritten as

$$\frac{d\sigma}{d\Omega} = \frac{1}{N_s A_{s,sc}(\theta)} \left\{ \frac{I_{sc}^*(\theta)}{a(\theta)} - \left[M_{sc}(\theta) - \frac{A_{c,sc}(\theta)}{A_{c,c}(\theta)} M_c(\theta) \right] \right\}. \quad (9)$$

In this equation the measured sample in container intensity, corrected for background and attenuated container scattering, is given by

$$I_{sc}^*(\theta) = [I_{sc}^E(\theta) - I_b^E(\theta)] - \frac{A_{c,sc}(\theta)}{A_{c,c}(\theta)} \{x[I_c^E(\theta) - I_b^E(\theta)] + (1-x) \times [I_{c'}^E(\theta) - I_b^E(\theta)]\} \equiv I_{sc}^E(\theta) - A_1(\theta) I_c^E(\theta) - A_2(\theta) I_{c'}^E(\theta) - A_3(\theta) I_b^E(\theta), \quad (10)$$

where the new terms are given by $A_1(\theta) = x A_{c,sc}(\theta)/A_{c,c}(\theta)$, $A_2(\theta) = (1-x) A_{c,sc}(\theta)/A_{c,c}(\theta)$, and $A_3(\theta) = 1 - A_{c,sc}(\theta)/A_{c,c}(\theta)$. In Eq. (10) it is assumed that the empty anvil measurement, $I_b^E(\theta)$, is representative of the background scattering for $I_{sc}^E(\theta)$, $I_c^E(\theta)$, and $I_{c'}^E(\theta)$. The coefficient x ($0 \le x \le 1$) in Eq. (10) is used to weight the background-corrected container scattering and is unity for an ambient-pressure experiment. For the GeO_2 samples investigated in the present work the ratio $A_{c,sc}(\theta)/A_{c,c}(\theta)$ did not have a strong 2θ dependence and, in practice, the angular dependence of the coefficients $A_m(\theta)$ ($m=1,2,3$) was neglected. Equation (9) was also used to correct the data measured for the vanadium standards.

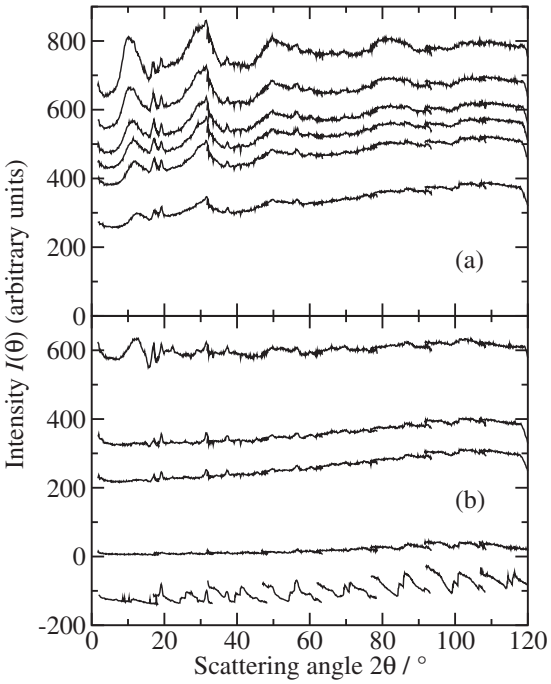

FIG. 5. The intensity $I(\theta)$ as a function of the scattering angle 2θ as measured in study B for, from top to bottom, (a) GeO_2 glass at ambient pressure, 2.2, 4.0, 4.9, 5.8, and 8.0 GPa and (b) the empty uncompressed Ti-Zr gasket, an empty Ti-Zr gasket recovered from 8.6 GPa with an applied load of 6.8 tonne, an empty Ti-Zr gasket recovered from 8.0 GPa with an applied load of 33.9 tonne, and the empty anvils with a spacing of 0.4 mm. The bottom curve in (b) is the empty anvil run from study A which is displaced vertically by 150 units for clarity of presentation. In an experiment on D4C the multidetector is moved to several fixed positions in order to cover the entire scattering angle range (Ref. 25). The stepping observed in the diffraction patterns, which is particularly pronounced for the empty anvil run from study A [bottom curve in (b)], arises from the change in background scattering that is observed for each position of the multidetector. In study B this stepping was significantly *reduced* by the incorporation of improved neutron shielding.

The measured intensities from study B for the GeO_2 glass at different pressures, three empty Ti-Zr gaskets under different conditions and the empty anvils are shown in Fig. 5. In the case of the empty gasket measurements, the Ti-Zr alloy has a mean coherent scattering length of zero so that the diffraction experiment amounts to a measurement of the Bhatia-Thornton[92] concentration-concentration partial structure factor, i.e., the observed structure, which is most evident at low pressures, arises from concentration fluctuations. A few small Bragg peaks occur at, e.g., $2\theta \simeq 17.1$, 19.2, 22.3, and 31.5° and the slope at larger scattering angles increases with pressure as the anvils close and more scattering is observed from the Cd shielding that covers them. At each pressure point, the weighting factor x in Eq. (10) was adjusted to ensure that these obvious contributions from the gasket and anvil scattering were eliminated from $I_{sc}^{E}(\theta)$. In practice, this sometimes meant that the associated coefficients $A_m(\theta)$ in Eq. (10) were allowed to vary from their ideal values, i.e., the $A_m(\theta)$ did not necessarily sum to unity. The measured intensity for the empty anvils in study A is also shown in Fig. 5(b). There is a considerable reduction in the background scattering for study B owing to the use of improved neutron shielding.

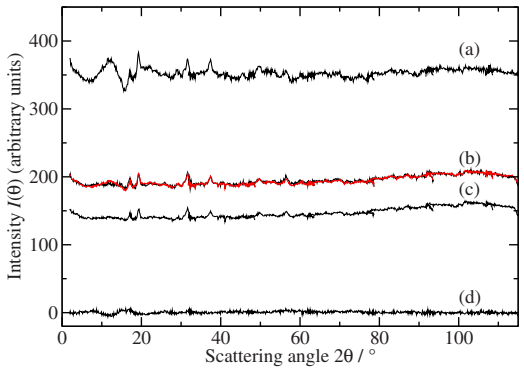

FIG. 6. (Color online) The intensity $I(\theta)$ as a function of the scattering angle 2θ as measured in a separate experiment (see the text) for a selection of empty Ti-Zr gaskets in the Paris-Edinburgh press. The black curve labeled (a) corresponds to the intensity $I_c^E(\theta)$ measured for an uncompressed gasket with an applied load of 6.8 tonne, the black curve labeled (b) corresponds to the intensity $I_{c'}^E(\theta)$ measured for a gasket recovered from 4.9(5) GPa with an applied load of 20.3 tonne and the black curve labeled (c) corresponds to the intensity $I_{c''}^E(\theta)$ measured for a gasket recovered from 8.0(5) GPa with an applied load of 33.9 tonne. The red curve labeled (b) gives the reconstruction of $I_{c'}^E(\theta)$ from the linear combination $I_{\rm rec}(\theta)=0.23I_c^E(\theta)+0.77I_{c''}^E(\theta)$. The black curve labeled (d) gives the difference function $I_{c'}^E(\theta)-I_{\rm rec}(\theta)$.

To make a closer examination of the linear approximation made in Eq. (10), a separate neutron-diffraction experiment was made in which the intensity was measured for a selection of empty Ti-Zr gaskets in the Paris-Edinburgh press. The intensity $I_c^E(\theta)$ was measured for an empty uncompressed Ti-Zr gasket, the intensity $I_{c'}^E(\theta)$ was measured for an empty Ti-Zr gasket recovered from 4.9(5) GPa and the intensity $I_{c''}^E(\theta)$ was measured for an empty Ti-Zr gasket recovered from 8.0(5) GPa. These intensities are illustrated in Fig. 6 along with the reconstruction of $I_{c'}^E(\theta)$ from the linear combination $I_{\rm rec}(\theta)=0.23I_c^E(\theta)+0.77I_{c''}^E(\theta)$ and the difference function $I_{c'}^E(\theta)-I_{\rm rec}(\theta)$. The results show that the main features of $I_{c'}^E(\theta)$ are reproduced by a linear combination of $I_c^E(\theta)$ and $I_{c''}^E(\theta)$. Future high-pressure work would benefit from a more complete investigation of the pressure dependence of the diffraction pattern for the Ti-Zr gasket alloy, e.g., to determine whether there is a phase transformation at a pressure in the range $\approx 6-11$ GPa as observed for elemental Ti, Zr, and the equiatomic alloy TiZr (see Sec. III B).

In the case of the ambient-pressure data set, the efficacy of the data-correction procedure could be readily assessed by comparison with the results obtained from a separate diffraction experiment on a bulk sample (see Sec. V).[14,15] Self-consistency checks were also made on all of the structure factors $S_{\rm N}(k)$ that were obtained from the corrected $F_{\rm N}(k)$ functions by using Eq. (4). It was checked that (i) each $S_{\rm N}(k)$ obeys the sum-rule relation $\int_0^\infty dk k^2[S_{\rm N}(k)-1]=-2\pi^2 n_0$ which follows from taking the small r limit of Eq. (5), (ii)

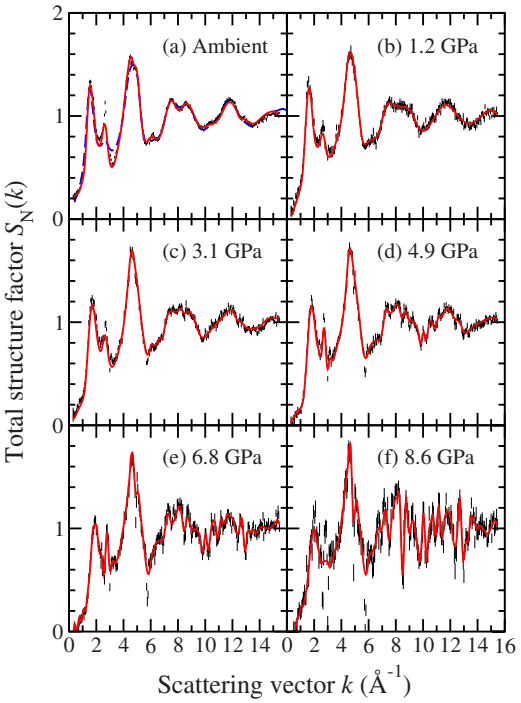

FIG. 7. (Color online) The total neutron structure factor $S_N(k)$ measured in study A for GeO_2 glass at (a) ambient pressure, (b) 1.2 GPa, (c) 3.1 GPa, (d) 4.9 GPa, (e) 6.8 GPa, and (f) 8.6 GPa. The vertical bars represent the measured data points with statistical errors and the solid (red) curves are the Fourier backtransforms of the corresponding total pair-distribution functions $G_N(r)$ given by the solid (black) curves in Fig. 9 after the unphysical oscillations at r values smaller than the distance of closest approach between the centers of two atoms are set to the calculated $G_N(r=0)=0$ limit. For reference, the broken (blue) curve in (a) gives the $S_N(k)$ function measured for a bulk sample of GeO_2 under ambient conditions by using the same neutron diffractometer but with an incident wavelength of 0.5 Å (Refs. 14 and 15).

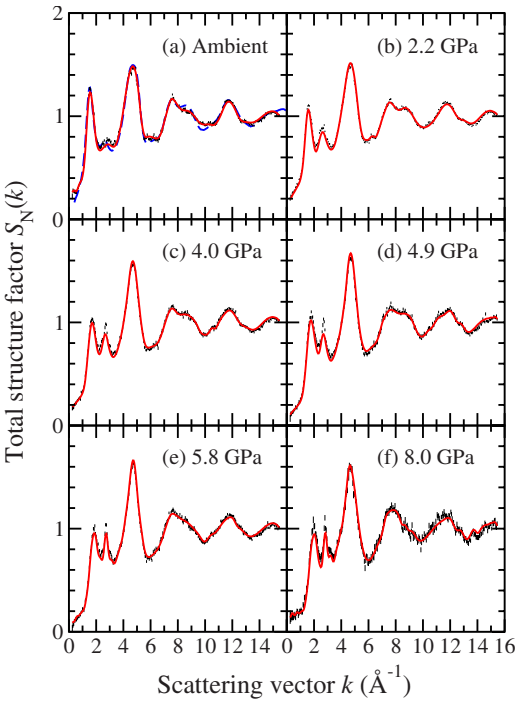

FIG. 8. (Color online) The total neutron structure factor $S_N(k)$ measured in study B for GeO_2 glass at (a) ambient pressure, (b) 2.2 GPa, (c) 4.0 GPa, (d) 4.9 GPa, (e) 5.8 GPa, and (f) 8.0 GPa. The vertical bars represent the measured data points with statistical errors and the solid (red) curves are the Fourier backtransforms of the corresponding total pair-distribution functions $G_N(r)$ given by the solid (black) curves in Fig. 10 after the unphysical oscillations at r values smaller than the distance of closest approach between the centers of two atoms are set to the calculated $G_N(r=0)=0$ limit. For reference, the broken (blue) curve in (a) gives the $S_N(k)$ function measured for a bulk sample of GeO_2 under ambient conditions by using the same neutron diffractometer but with an incident wavelength of 0.5 Å (Refs. 14 and 15).

the low-r features in $G_N(r)$ oscillate about the correct $G_N(r=0)=0$ limit, and (iii) the Fourier backtransform of $G_N(r)$ with the low-r oscillations set to the $G_N(0)$ limit is in good overall agreement with the measured $S_N(k)$ function.[87]

V. RESULTS

The total structure factors $S_N(k)$ measured for glassy GeO_2 in studies A and B at pressures up to 8.6(5) GPa are illustrated in Figs. 7 and 8, respectively. The corresponding total pair-correlation functions are shown in Figs. 9 and 10. Several of the parameters describing the structure are listed in Table I. The results from study B show a significant improvement in the quality of the data, especially at high pressures, which was achieved mainly from a reduction in the background scattering. In Figs. 7(a) and 8(a) the structure factor measured for the glass in the Paris-Edinburgh press at ambient pressure is compared with the $S_N(k)$ function measured for a bulk sample of GeO_2 glass at ambient pressure using the same neutron diffractometer D4C with an incident neutron wavelength of 0.5 Å.[14,15] The ambient-pressure data sets are in agreement within the experimental error at most k values which supports the efficacy of the data-reduction procedure. The discrepancy in Fig. 7(a) between the Paris-Edinburgh press and bulk sample data in the region around 2–3 Å^{-1} is attributed mainly to a difficulty in accounting for a step in the background intensity in the detector overlap region between ≈2.6–2.9 Å^{-1} [see Fig. 5(b)] although there is evidence for a small amount of Bragg scattering from the sample arising from the procedure used to anneal the glass (see Sec. III A). The first sharp diffraction peak (FSDP) position at ≃1.53 Å^{-1} is in agreement with the results given in Refs. 14 and 15 indicating that the method used to precompress the powder pellet for the Paris-Edinburgh press had little observable effect on the structure of the illuminated portion of the glass.

The pressure dependence of the position of the FSDP, k_{FSDP}, in the total structure factor is shown in Fig. 11 where a comparison is also made with the results obtained from the x-ray diffraction studies of Guthrie *et al.*[9] and Hong *et al.*[21] The data show a steady increase in k_{FSDP} with pressure. This is consistent with a steady compaction of the intermediate range atomic ordering which has a periodicity in r space given by $2\pi/k_{FSDP}$.[93] Under ambient conditions the principal

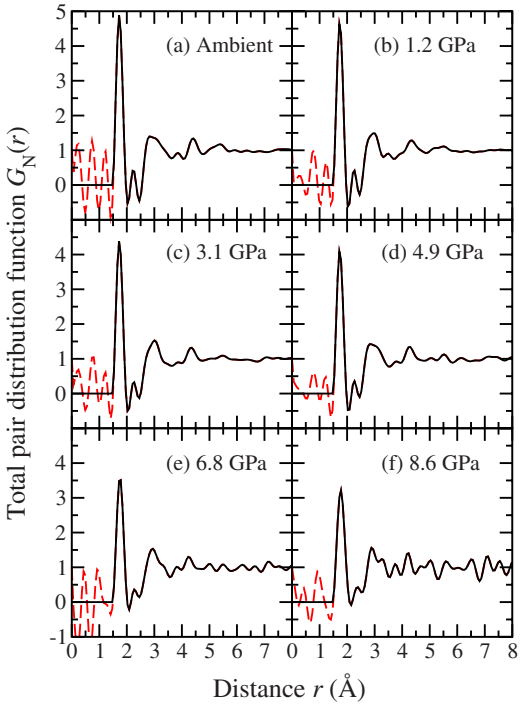

FIG. 9. (Color online) The total neutron pair-distribution function $G_N(r)$ measured in study A for GeO_2 glass at (a) ambient pressure, (b) 1.2 GPa, (c) 3.1 GPa, (d) 4.9 GPa, (e) 6.8 GPa, and (f) 8.6 GPa [solid (black) curves] as obtained by Fourier transforming the corresponding $S_N(k)$ function given by the vertical bars in Fig. 7 after spline fitting and truncating at $k_{max}=15.45$ Å^{-1}. The broken (red) curves show the extent of the unphysical oscillations at r values smaller than the distance of closest approach between the centers of two atoms.

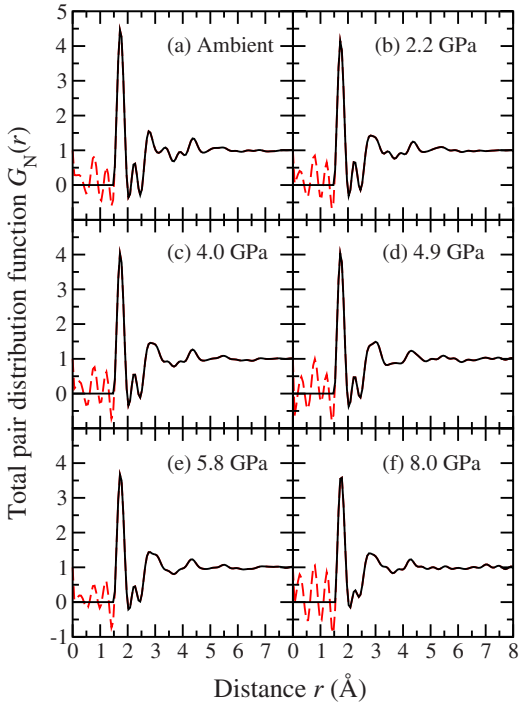

FIG. 10. (Color online) The total neutron pair-distribution function $G_N(r)$ measured in study B for GeO_2 glass at (a) ambient pressure, (b) 2.2 GPa, (c) 4.0 GPa, (d) 4.9 GPa, (e) 5.8 GPa, and (f) 8.0 GPa [solid (black) curves] as obtained by Fourier transforming the corresponding $S_N(k)$ function given by the vertical bars in Fig. 8 after spline fitting and truncating at $k_{max}=15.45$ Å^{-1}. The broken (red) curves show the extent of the unphysical oscillations at r values smaller than the distance of closest approach between the centers of two atoms.

and third peaks in $S_N(k)$ appear at 2.67(2) and 4.70(2) Å^{-1}, respectively.[14,15] The principal peak becomes an increasingly sharp feature with increasing pressure while the height of the third peak increases. These general trends are in keeping with those found from neutron-diffraction experiments on samples that had been compacted at different pressures, heat treated at 673 K for 2 min under load, and recovered to ambient conditions.[17,34] At ambient pressure, Fig. 9 of Ref. 15 shows that the Ge-O and Ge-Ge correlations give the largest contribution to the FSDP in $S_X(k)$ and that there is a negligible contribution from the O-O correlations. By comparison, Fig. 10 of Ref. 15 shows that the Ge-O correlations give the major contribution to the FSDP in $S_N(k)$ at ambient pressure and that there are smaller contributions from the Ge-Ge and O-O correlations. It is therefore likely that the changes observed with increasing pressure in the FSDP region for $S_N(k)$ and $S_X(k)$ are associated with changes in the Ge atom correlations, a viewpoint supported by several molecular-dynamics simulations.[40,41] For example, since the Ge-Ge correlations correspond to those between the centers of the structural motifs, the FSDP position in $S_{GeGe}(k)$ is anticipated to move to larger k values with increasing pressure as the network compacts. It is notable that Sampath *et al.*[18] made a joint neutron and x-ray diffraction study on GeO_2 glass recovered to ambient conditions from 10 GPa and found that the changes in the FSDP region are least

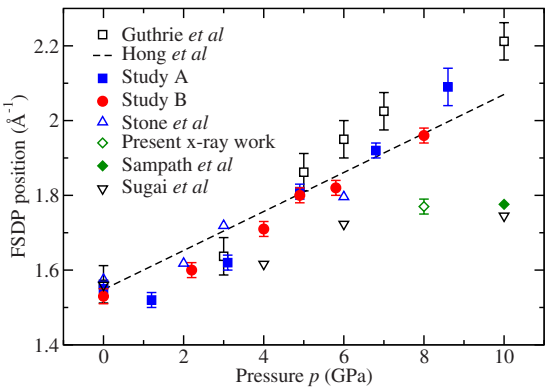

FIG. 11. (Color online) Pressure dependence of the FSDP position, k_{FSDP}, in $S_N(k)$ or $S_X(k)$ for GeO_2 glass. The results obtained from the *in situ* neutron-diffraction studies A [(blue) ■] and B [(red) ●] of the present work are given together with the results obtained from the *in situ* x-ray diffraction studies of Guthrie *et al.* (Ref. 9) (□) and Hong *et al.* (Ref. 21) (broken curve). Also shown are the results obtained for samples densified at the indicated pressures and recovered to ambient conditions from the neutron-diffraction work of Stone *et al.* (Ref. 17) [(blue) △] and from the x-ray diffraction work of the present paper [(green) ◇], Sampath *et al.* (Ref. 18) [(green) ◆] and Sugai and Onodera (Ref. 33) (▽).

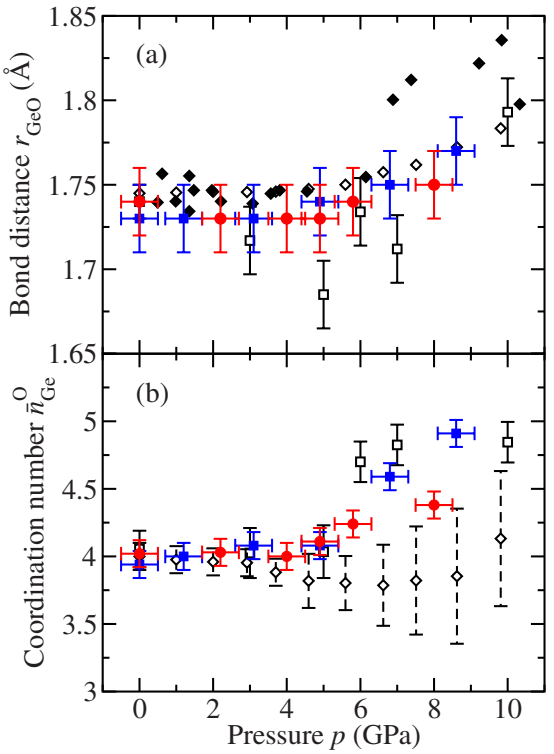

FIG. 12. (Color online) The pressure dependence of (a) the nearest-neighbor peak position r_{GeO} in $G_N(r)$ and (b) the mean coordination number $\bar{n}^{O}_{Ge}$ for GeO_2 glass as measured in neutron-diffraction studies A [(blue) ■] and B [(red) ●] of the present work. The $\bar{n}^{O}_{Ge}$ values were found by integrating to the first minimum in the $G_N(r)$ function obtained by Fourier transforming $S_N(k)$ after applying a Lorch (Ref. 94) modification function with k_{max} = 15.45 Å^{-1} (see the text). Also shown are the results obtained from the x-ray diffraction study of Guthrie *et al.* (Ref. 9) (□), the EXAFS study of Vaccari *et al.* (Ref. 12) (◇), and the EXAFS study of Itié *et al.* (Ref. 5) (◆). The reported accuracy of the r_{GeO} distances in Refs. 5 and 12 are 0.015 and 0.01 Å, respectively.

pronounced with respect to the Ge-Ge correlations, i.e., the Ge-O correlations presumably play an important role.

The first peak in $G_N(r)$ is attributed to nearest-neighbor Ge-O correlations by comparison with the partial pair-distribution functions measured for the glass at ambient pressure by applying the method of isotope substitution in neutron diffraction.[14,15] The pressure dependence of the Ge-O bond distance r_{GeO} and corresponding coordination number is illustrated in Fig. 12. The coordination numbers were obtained by applying a Lorch[94] modification function (with a maximum value k_{max}=15.45 Å^{-1}) to $S_N(k)$, Fourier transforming, and then integrating over the first peak in the resultant $G_N(r)$ function up to the first minimum [see Eq. (3)]. These $\bar{n}^{O}_{Ge}$ values are, within the quoted error, the same as those obtained by finding the first plateau in the running coordination number[95] calculated by using the first peak in the $G_N(r)$ functions shown in Figs. 9 and 10. In addition, the Ge-O coordination number was obtained by using the method described in Ref. 15 where the first peak in $d_{GeO}(r) \equiv 4\pi n_0 r[g_{GeO}(r)-1]$, assumed to be a single Gaussian function, was convoluted with the Fourier transform of the step modification function $M(k \leq k_{max})=1$, $M(k>k_{max})=0$ with k_{max}=15.45 Å^{-1} and fitted to the first peak in each measured $G_N(r)$ function. The $\bar{n}^{O}_{Ge}$ values thus obtained have the same pressure dependence as shown in Fig. 12, although the absolute values are on average ≃0.15 smaller. This difference may result, in part, from the effect of errors on $S_N(k)$ in the region of the first peak in r space. Notwithstanding, the results show little change in the local coordination environment of Ge until a pressure of ≈ 5 GPa is achieved. A steady increase in the coordination number to $\bar{n}^{O}_{Ge}$=4.9(1) at 8.6(5) GPa is then observed as r_{GeO} increases, i.e., the first coordination shell of Ge expands in order to accommodate an increased number of nearest neighbors.

In Fig. 12 the r_{GeO} and $\bar{n}^{O}_{Ge}$ values obtained from neutron-diffraction studies A and B are compared with the results found from other *in situ* high-pressure studies of GeO_2 glass using both high-energy x-ray diffraction[9] and extended x-ray absorption fine-structure (EXAFS) spectroscopy.[5,12] The Ge-O bond distances obtained from neutron diffraction are in general agreement with the values obtained from the recent EXAFS study of Vaccari *et al.*[12] but there is a discrepancy at pressures ≳6 GPa between these data sets and the values reported in the earlier EXAFS work of Itié *et al.*[5] A gradual change in r_{GeO} with increasing pressure is also reported from EXAFS experiments on GeO_2 gel prepared by the hydrolysis of $GeCl_4$.[35] The coordination numbers obtained from diffraction are in good accord but the mean values obtained by Vaccari *et al.*[12] are somewhat smaller at higher pressures. According to these authors, a discrepancy may arise from the difficulty in treating the amplitude of EXAFS signals measured in high-pressure experiments. We note that the x-ray diffraction results of Guthrie *et al.*[9] suggested a plateau in the pressure dependence of the Ge-O coordination number between about 7 and 10 GPa [their data points are given in Fig. 12(b)]. It is not possible to confirm the existence of this plateau from the spread in coordination numbers shown in Fig. 12(b). However, the Ge-O bond distances shown in Fig. 12(a) are consistent with a steady increase in the coordination number over this pressure range as the first coordination shell of Ge expands to accommodate a larger number of nearest neighbors.

At ambient pressure, the measured partial pair-distribution functions for GeO_2 glass show that the nearest-neighbor O-O distance is shorter than the nearest-neighbor Ge-Ge distance.[14,15] The second peak position at r_2 in $G_N(r)$ is therefore assigned to oxygen-oxygen correlations and, for regular tetrahedral GeO_4 units, the ratio $r_{OO}/r_{GeO}=\sqrt{8/3}$ =1.633. The ratio calculated from the measured partial pair-distribution functions for GeO_2 glass under ambient conditions is 1.636(11) (Ref. 15) and it is anticipated to show a significant change with increasing pressure.[40] The ratio calculated from the data given in Table I does not, however, display a pressure-dependent systematic trend despite the increase shown in the Ge-O coordination number at elevated pressures. This may result from an increasing overlap with pressure between the nearest-neighbor O-O and Ge-Ge correlations that renders unsafe the assignment of r_2 solely to O-O correlations. It is not possible to resolve the nearest-neighbor Ge-Ge distance in the measured $G_N(r)$ functions so changes with pressure in the Ge-Ô-Ge bond

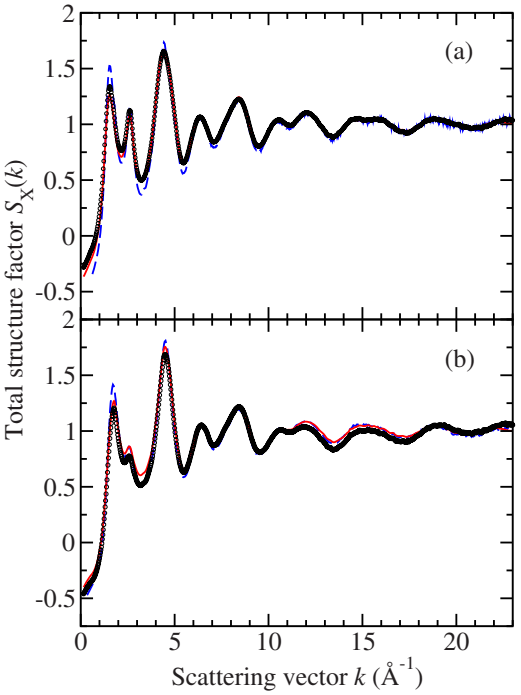

FIG. 13. (Color online) The total x-ray structure factor $S_X(k)$ measured for GeO_2 glass when (a) uncompressed and (b) recovered from 8.0 GPa after neutron-diffraction study B. The black circles give the measured data points and the solid (red) curves are the Fourier backtransforms of the corresponding $G_X(r)$ functions given in Fig. 14 after the unphysical oscillations at r values smaller than the distance of closest approach between the centers of two atoms are set to the calculated $G_X(r=0)=0$ limit. The broken (blue) curves give the $S_X(k)$ functions measured for GeO_2 glass by Sampath *et al.* (Ref. 18) for (a) the uncompressed material and (b) the material recovered from 10 GPa.

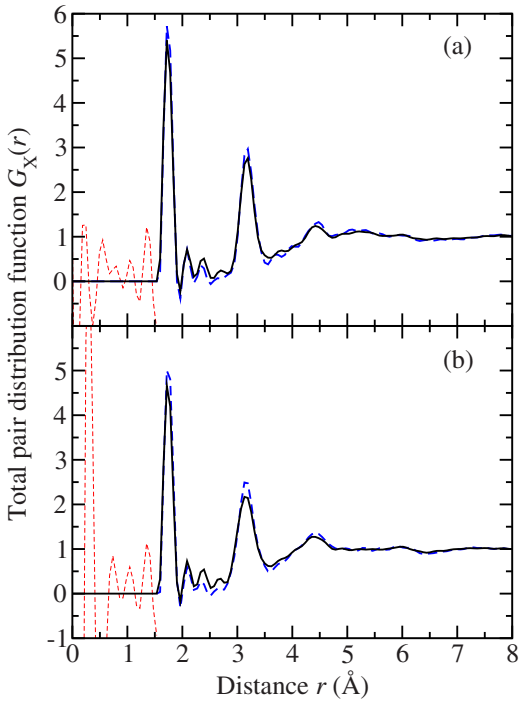

FIG. 14. (Color online) The total x-ray pair-distribution function $G_X(r)$ measured for GeO_2 glass when (a) uncompressed and (b) recovered from 8.0 GPa after neutron-diffraction study B. The solid (black) curves were obtained by Fourier transforming the corresponding $S_X(k)$ functions given by the circles in Fig. 13 after spline fitting and smoothly truncating by applying a cosine window function over the range $21 \leq k(\text{Å}^{-1}) \leq 23$. The broken (blue) curves give the $G_X(r)$ functions for GeO_2 glass obtained by Fourier transforming the $S_X(k)$ functions of Sampath *et al.* (Ref. 18) given in Fig. 13 after truncating at $k_{max}=23$ Å^{-1} for (a) the uncompressed material and (b) the material recovered from 10 GPa.

angle from its ambient value of $\simeq 132(2)°$ could not be observed.[14,15,62,96–98]

At the end of study B the GeO_2 glass was recovered from 8.0(5) GPa and, a few hours later, it was studied by using high-energy x-ray diffraction. A piece of the corresponding as-prepared GeO_2 glass was also investigated. The number density of the uncompressed glass is 0.0629(3) Å^{-3} (Ref. 15) and a number density of 0.0694 Å^{-3} for the recovered glass was taken from the density data shown in Fig. 3. The measured total structure factors $S_X(k)$ are shown in Fig. 13 and the corresponding total pair-distribution functions $G_X(r)$ are given in Fig. 14. The data in these figures is compared with the high-energy x-ray diffraction results of Sampath *et al.*[18] The FSDP in $S_X(k)$ appears at 1.54(2) Å^{-1} for the uncompressed sample and at 1.77(2) Å^{-1} for the recovered sample (see Fig. 11).

The mean Ge-O coordination number was obtained by first Fourier transforming the function ${}^{\text{mod}}S_X(k)-1 \equiv F_X(k)/\{2c_{Ge}c_O f_{Ge}(k)f_O(k)\}$ to remove the k-dependent atomic form factors that otherwise weight the Ge-O partial structure factor.[68] The resultant r space function was then written in the form ${}^{\text{mod}}D_X(r)=4\pi n_0 r[{}^{\text{mod}}G_X(r)-1]$ so that within the first peak region the function $d_{GeO}(r)=4\pi n_0 r[g_{GeO}(r)-1]$ is given by $d_{GeO}(r) = {}^{\text{mod}}D_X(r)+4\pi n_0 r\{[c_{Ge}^2 f_{Ge}^2(k=0)+c_O^2 f_O^2(k=0)]/2c_{Ge}c_O f_{Ge}(k=0)f_O(k=0)\}$. The effect of the finite extent of the diffractometer measurement window was then taken into account by fitting the first peak in this function by using a single Gaussian convoluted with the Fourier transform of the step modification function $M(k \leq k_{max})=1$, $M(k>k_{max})=0$ with $k_{max}=23$ Å^{-1}. The resultant fits gave $\bar{n}_{Ge}^{O}=3.9(1)$ for both the uncompressed and recovered samples corresponding to peak positions of 1.73(2) and 1.74(2) Å in $g_{GeO}(r)$, respectively. We note that, in view of the uncertainty in the time scale for relaxation of GeO_2 glass on release of an applied pressure and the study by x-ray diffraction of the sample a few hours after decompression, the x-ray data for the sample recovered from 8 GPa was also analyzed by assuming a number density of 0.0773 Å^{-3} which lies between the *in situ* and recovered values shown in Fig. 3. The results gave $\bar{n}_{Ge}^{O}=4.0(1)$ with a peak position of 1.74(2) Å in $g_{GeO}(r)$.

VI. DISCUSSION

At pressures up to ≈ 5 GPa there is no observable change in the mean nearest-neighbor Ge-O coordination number or corresponding distance r_{GeO} (see Fig. 12) but there is a continuous change in position and height of the FSDP in the total structure factor $S_N(k)$ (see Fig. 11). As the pressure is

increased beyond 5 GPa, however, there is also an increase in the mean Ge-O coordination number from 4 to 4.9(1) at 8.6(5) GPa. The results are therefore consistent with the operation of two compaction mechanisms.[9,44] At low pressures there is a reorganization of the GeO_4 tetrahedra which manifests itself in the FSDP as a change in the intermediate range order. Within this regime, Raman spectroscopy results[6,13] have been interpreted in terms of a reduction in the mean intertetrahedral Ge-$\hat{O}$-Ge bond angle accompanied by a distortion of the GeO_4 tetrahedra which manifests itself in terms of a larger distribution of intratetrahedral O-$\hat{Ge}$-O angles rather than by a change in the Ge-O bond length. This type of behavior is observed for the α-quartzlike form of crystalline GeO_2 (Refs. 99 and 100) which the glass is thought to resemble.[62,101] At higher pressures, further reorganization of the intermediate range order is facilitated by an increase in the local coordination number. *In situ* Raman and Brillouin spectroscopy studies of GeO_2 glass suggest a change in the compression mechanism at pressures above $\simeq 4$ GPa.[6,13,32]

When GeO_2 glass is recovered from pressures up to 10 GPa, the present and other x-ray and neutron-diffraction[17,18] experiments show that the Ge-O coordination number returns to 4. For compaction pressures up to $\simeq$ 4 GPa, the recovered and *in situ* sample densities are comparable (see Fig. 3) and the first sharp diffraction peaks occur at a comparable position (see Fig. 11). These observations can be rationalized on the basis that the data points for the recovered glass within this pressure regime correspond to samples that had been heated at 673 K for 2 min under load before recovery to ambient conditions,[17,34] i.e., it is likely that thermal relaxation under pressure led to samples that were originally denser than those studied *in situ* at the same pressure but at room temperature with elastic expansion of the material on pressure release leading to lower densities that are comparable to the *in situ* values. The recovered glass is, therefore, permanently densified and there are similarities in the local and intermediate range ordering for the recovered and *in situ* samples. Neutron-diffraction experiments on glasses compacted at pressures up to 6 GPa and recovered to ambient conditions show a small increase in the Ge-O bond length from 1.733(1) to 1.739(1) Å and a reduction in the mean intertetrahedral Ge-$\hat{O}$-Ge bond angle with increasing density.[17] However, for compaction pressures $\gtrsim$5 GPa, the density and FSDP position for the recovered glass are smaller than their *in situ* values (see Figs. 3 and 11) and the mean Ge-O coordination number $\bar{n}_{Ge}^{O} \simeq$ 4 for the recovered glass is smaller than the *in situ* values, i.e., there is a reorganization of both the local and intermediate range ordering once the pressure is released. As shown in Fig. 12 this change in behavior coincides with the pressure at which the tetrahedral ordering begins to break for the samples studied *in situ*.

A mean Ge-O coordination number greater than four at high-pressure suggests the coexistence of GeO_4 tetrahedra with GeO_5 polyhedra, GeO_6 octahedra or, indeed, a mixture of all three types of structural unit. This assignment is supported by the increase in Ge-O bond length from r_{GeO} = 1.73(2) Å at ambient pressure to 1.77(2) Å at 8.6(5) GPa. For example, the Ge-O bond length for tetrahedral GeO_4 units in the glass is 1.73(1) Å.[10,14,15,17,62,97,101] Several crystal structures have GeO_5 polyhedra[102] which occur in the form of trigonal bipyramids, as in the case of $K_2Ge_8O_{17}$,[103,104] or in the form of square pyramids. For the trigonal bipyramids there are shorter equatorial Ge-O bonds of length $\simeq$1.70–1.80 Å and longer axial Ge-O bonds of length $\simeq$1.89–1.99 Å while for the square pyramids the Ge-O bond lengths are in the range $\simeq$1.76–1.96 Å. The possibility of GeO_5 polyhedra in germanate glasses has also been reported with Ge-O bond lengths in the range 1.75–1.93 Å.[102,105,106] The mean Ge-O bond length for GeO_6 octahedra in the rutile phase of crystalline germania is 1.88 Å at ambient pressure[102] and 1.85 Å at 16 GPa.[107] The occurrence of GeO_5 units in germania liquid and glass with increasing pressure is supported by several molecular-dynamics simulations.[9,43,44,46,49] Their presence cannot, however, be unambiguously inferred from the present data sets.

VII. CONCLUSIONS

The results show that GeO_2 glass exhibits a threshold pressure $p_{th} \simeq 5$ GPa about which the material shows different structural properties. At pressures extending from ambient to p_{th} the density and structure of the material studied *in situ* is similar to that of the permanently densified glass recovered from high pressure. There is a change in the intermediate range ordering which is associated with a reorganization of GeO_4 tetrahedra as the mean intertetrahedral Ge-$\hat{O}$-Ge bond angle reduces. When the pressure is increased from p_{th} to 8.6(5) GPa, the *in situ* diffraction studies show a continuous increase with pressure in the Ge-O coordination number from 4 to 4.9(1) and the corresponding bond length increases from 1.73(2) to 1.77(2) Å as the first coordination shell of germanium expands in order to accept an increased number of oxygen nearest neighbors. The observed pressure dependence of the Ge-O bond length matches the results found in the recent EXAFS study of Vaccari *et al.*[12] When the glass is recovered to ambient from pressures above p_{th} the density reduces and the intermediate range ordering adjusts as the Ge-O coordination number returns to a value of 4. It will be interesting to follow this reorganization at higher pressures on formation of the octahedral glass and to follow the time dependence of the relaxation processes.

ACKNOWLEDGMENTS

We thank Pierre Palleau, Alain Bertoni, Jean-Luc Laborier, and Claude Payre for help with the D4C experiments, Alexei Bytchkov for help with the ID11 experiment, Chris Benmore (ANL) and Malcolm Guthrie (APS) for useful discussions, Punit Boolchand (Cincinnati) for advice on the MDSC experiments, and Duncan Francis (ISIS Facility) for providing us with Ti-Zr gaskets. Anita Zeidler and Dean Whittaker are thanked for their help in providing the data shown in Fig. 6.

[1] C. A. Angell, Science **267**, 1924 (1995).
[2] S. Ono, T. Tsuchiya, K. Hirose, and Y. Ohishi, Phys. Rev. B **68**, 134108 (2003).
[3] V. P. Prakapenka, G. Shen, L. S. Dubrovinsky, M. L. Rivers, and S. R. Sutton, J. Phys. Chem. Solids **65**, 1537 (2004).
[4] Q. Williams and R. Jeanloz, Science **239**, 902 (1988).
[5] J. P. Itié, A. Polian, G. Calas, J. Petiau, A. Fontaine, and H. Tolentino, Phys. Rev. Lett. **63**, 398 (1989).
[6] D. J. Durben and G. H. Wolf, Phys. Rev. B **43**, 2355 (1991).
[7] M. Madon, Ph. Gillet, Ch. Julien, and G. D. Price, Phys. Chem. Miner. **18**, 7 (1991).
[8] C. Meade, R. J. Hemley, and H. K. Mao, Phys. Rev. Lett. **69**, 1387 (1992).
[9] M. Guthrie, C. A. Tulk, C. J. Benmore, J. Xu, J. L. Yarger, D. D. Klug, J. S. Tse, H.-k. Mao, and R. J. Hemley, Phys. Rev. Lett. **93**, 115502 (2004).
[10] M. Micoulaut, L. Cormier, and G. S. Henderson, J. Phys.: Condens. Matter **18**, R753 (2006).
[11] T. Sato and N. Funamori, Phys. Rev. Lett. **101**, 255502 (2008).
[12] M. Vaccari, G. Aquilanti, S. Pascarelli, and O. Mathon, J. Phys.: Condens. Matter **21**, 145403 (2009).
[13] C. H. Polsky, K. H. Smith, and G. H. Wolf, J. Non-Cryst. Solids **248**, 159 (1999).
[14] P. S. Salmon, A. C. Barnes, R. A. Martin, and G. J. Cuello, Phys. Rev. Lett. **96**, 235502 (2006).
[15] P. S. Salmon, A. C. Barnes, R. A. Martin, and G. J. Cuello, J. Phys.: Condens. Matter **19**, 415110 (2007).
[16] Q. Mei, C. J. Benmore, S. Sen, R. Sharma, and J. L. Yarger, Phys. Rev. B **78**, 144204 (2008).
[17] C. E. Stone, A. C. Hannon, T. Ishihara, N. Kitamura, Y. Shirakawa, R. N. Sinclair, N. Umesaki, and A. C. Wright, J. Non-Cryst. Solids **293-295**, 769 (2001).
[18] S. Sampath, C. J. Benmore, K. M. Lantzky, J. Neuefeind, K. Leinenweber, D. L. Price, and J. L. Yarger, Phys. Rev. Lett. **90**, 115502 (2003).
[19] D. J. Lacks, Phys. Rev. Lett. **84**, 4629 (2000).
[20] V. V. Brazhkin and A. G. Lyapin, J. Phys.: Condens. Matter **15**, 6059 (2003).
[21] X. Hong, G. Shen, V. B. Prakapenka, M. Newville, M. L. Rivers, and S. R. Sutton, Phys. Rev. B **75**, 104201 (2007).
[22] P. S. Salmon, R. A. Martin, P. E. Mason, and G. J. Cuello, Nature (London) **435**, 75 (2005).
[23] P. S. Salmon, J. Phys.: Condens. Matter **17**, S3537 (2005).
[24] P. S. Salmon, J. Phys.: Condens. Matter **19**, 455208 (2007).
[25] H. E. Fischer, G. J. Cuello, P. Palleau, D. Feltin, A. C. Barnes, Y. S. Badyal, and J. M. Simonson, Appl. Phys. A: Mater. Sci. Process. **74**, S160 (2002).
[26] K. Tanaka, Philos. Mag. Lett. **57**, 183 (1988).
[27] L. Červinka, J. Non-Cryst. Solids **106**, 291 (1988).
[28] T. Yamanaka, K. Sugiyama, and K. Ogata, J. Appl. Crystallogr. **25**, 11 (1992).
[29] S. Kawasaki, O. Ohtaka, and T. Yamanaka, Phys. Chem. Miner. **20**, 531 (1994).
[30] S. K. Sharma, D. Virgo, and I. Kushiro, J. Non-Cryst. Solids **33**, 235 (1979).
[31] K. Suito, M. Miyoshi, T. Sasakura, and H. Fujisawa, in *High-Pressure Research: Applications to Earth and Planetary Sciences*, edited by Y. Syono and M. H. Manghnani (American Geophysical Union, Washington, DC, 1992), p. 219.
[32] G. H. Wolf, S. Wang, C. A. Herbst, D. J. Durben, W. F. Oliver, Z. C. Kang, and K. Halvorson, in *High-Pressure Research: Applications to Earth and Planetary Sciences*, edited by Y. Syono and M. H. Manghnani (American Geophysical Union, Washington, DC, 1992), p. 503.
[33] S. Sugai and A. Onodera, Phys. Rev. Lett. **77**, 4210 (1996).
[34] T. Ishihara, Y. Shirakawa, T. Iida, N. Kitamura, M. Matsukawa, N. Ohtori, and N. Umesaki, Jpn. J. Appl. Phys., Part 1 **38**, 3062 (1999).
[35] O. Ohtaka, A. Yoshiasa, H. Fukui, K. Murai, M. Okube, H. Takebe, Y. Katayama, and W. Utsumi, J. Phys.: Condens. Matter **14**, 10521 (2002).
[36] R. D. Oeffner and S. R. Elliott, Phys. Rev. B **58**, 14791 (1998).
[37] T. Tsuchiya, T. Yamanaka, and M. Matsui, Phys. Chem. Miner. **25**, 94 (1998).
[38] T. Tsuchiya, T. Yamanaka, and M. Matsui, Phys. Chem. Miner. **27**, 149 (2000).
[39] G. Gutiérrez and J. Rogan, Phys. Rev. E **69**, 031201 (2004).
[40] M. Micoulaut, J. Phys.: Condens. Matter **16**, L131 (2004).
[41] M. Micoulaut, Y. Guissani, and B. Guillot, Phys. Rev. E **73**, 031504 (2006).
[42] V. V. Hoang, J. Phys.: Condens. Matter **18**, 777 (2006).
[43] K. V. Shanavas, N. Garg, and S. M. Sharma, Phys. Rev. B **73**, 094120 (2006).
[44] M. Micoulaut, X. Yuan, and L. W. Hobbs, J. Non-Cryst. Solids **353**, 1961 (2007).
[45] A. Takada, P. Richet, C. R. A. Catlow, and G. D. Price, J. Non-Cryst. Solids **353**, 1892 (2007).
[46] P. K. Hung, L. T. Vinh, and D. M. Nghiep, J. Non-Cryst. Solids **353**, 2163 (2007).
[47] J. Peralta, G. Gutiérrez, and J. Rogan, J. Phys.: Condens. Matter **20**, 145215 (2008).
[48] M. Hawlitzky, J. Horbach, S. Ispas, M. Krack, and K. Binder, J. Phys.: Condens. Matter **20**, 285106 (2008).
[49] T. Li, S. Huang, and J. Zhu, Chem. Phys. Lett. **471**, 253 (2009).
[50] D. Marrocchelli, M. Salanne, P. A. Madden, C. Simon, and P. Turq, Mol. Phys. **107**, 443 (2009).
[51] L. Giacomazzi, P. Umari, and A. Pasquarello, Phys. Rev. Lett. **95**, 075505 (2005).
[52] L. Giacomazzi, P. Umari, and A. Pasquarello, Phys. Rev. B **74**, 155208 (2006).
[53] H. E. Fischer, A. C. Barnes, and P. S. Salmon, Rep. Prog. Phys. **69**, 233 (2006).
[54] T. E. Faber and J. M. Ziman, Philos. Mag. **11**, 153 (1965).
[55] V. F. Sears, Neutron News **3**, 26 (1992).
[56] N. Terakado and K. Tanaka, J. Non-Cryst. Solids **352**, 3815 (2006).
[57] T. M. Gross and M. Tomozawa, J. Non-Cryst. Solids **353**, 4762 (2007).
[58] A. V. Anan'ev, V. N. Bogdanov, B. Champagnon, M. Ferrari, G. O. Karapetyan, L. V. Maksimov, S. N. Smerdin, and V. A. Solovyev, J. Non-Cryst. Solids **354**, 3049 (2008).
[59] T. J. Kiczenski, C. Ma, E. Hammarsten, D. Wilkerson, M. Affatigato, and S. Feller, J. Non-Cryst. Solids **272**, 57 (2000).
[60] C. A. Angell and J. C. Tucker, in *Physical Chemistry of Process Metallurgy: The Richardson Conference* edited by J. H. E. Jeffes and R. J. Tait (Institute of Mining and Metallurgy, London, 1974), p. 207.
[61] A. Napolitano and P. B. Macedo, J. Res. Natl. Bur. Stand., Sect. A **72**, 425 (1968).
[62] A. J. Leadbetter and A. C. Wright, J. Non-Cryst. Solids **7**, 37

(1972).
[63] D. B. Dingwell, R. Knoche, and S. L. Webb, Phys. Chem. Miner. **19**, 445 (1993).
[64] S. Klotz, Th. Strässle, G. Rousse, G. Hamel, and V. Pomjakushin, Appl. Phys. Lett. **86**, 031917 (2005).
[65] C. L. Bull, M. Guthrie, S. Klotz, J. Philippe, Th. Strässle, R. J. Nelmes, J. S. Loveday, and G. Hamel, High Press. Res. **25**, 229 (2005).
[66] H. Bertagnolli, P. Chieux, and M. D. Zeidler, Mol. Phys. **32**, 759 (1976).
[67] S. Klotz, B. Padmanabhan, J. Philippe, and Th. Strässle, High Press. Res. **28**, 621 (2008).
[68] A. Zeidler, J. W. E. Drewitt, P. S. Salmon, A. C. Barnes, W. A. Crichton, S. Klotz, H. E. Fischer, C. J. Benmore, S. Ramos, and A. C. Hannon, J. Phys.: Condens. Matter **21**, 474217 (2009).
[69] X. Hong, G. Shen, V. B. Prakapenka, M. L. Rivers, and S. R. Sutton, Rev. Sci. Instrum. **78**, 103905 (2007).
[70] K. H. Smith, E. Shero, A. Chizmeshya, and G. H. Wolf, J. Chem. Phys. **102**, 6851 (1995).
[71] O. B. Tsiok, V. V. Brazhkin, A. G. Lyapin, and L. G. Khvostantsev, Phys. Rev. Lett. **80**, 999 (1998).
[72] H. M. Cohen and R. Roy, J. Am. Ceram. Soc. **44**, 523 (1961).
[73] H. M. Cohen and R. Roy, Phys. Chem. Glasses **6**, 149 (1965).
[74] Y. K. Vohra and P. T. Spencer, Phys. Rev. Lett. **86**, 3068 (2001).
[75] Y. Akahama, H. Kawamura, and T. Le Bihan, J. Phys.: Condens. Matter **14**, 10583 (2002).
[76] B. Olinger and J. C. Jamieson, High Temp.-High Press. **5**, 123 (1973).
[77] H. Xia, S. J. Duclos, A. L. Ruoff, and Y. K. Vohra, Phys. Rev. Lett. **64**, 204 (1990).
[78] Y. Akahama, M. Kobayashi, and H. Kawamura, J. Phys. Soc. Jpn. **60**, 3211 (1991).
[79] C. W. Greeff, Modell. Simul. Mater. Sci. Eng. **13**, 1015 (2005).
[80] Y. Zhao, J. Zhang, C. Pantea, J. Qian, L. L. Daemen, P. A. Rigg, R. S. Hixson, G. T. Gray, Y. Yang, L. Wang, Y. Wang, and T. Uchida, Phys. Rev. B **71**, 184119 (2005).
[81] I. O. Bashkin, V. K. Fedotov, M. V. Nefedova, V. G. Tissen, E. G. Ponyatovsky, A. Schiwek, and W. B. Holzapfel, Phys. Rev. B **68**, 054401 (2003).
[82] V. P. Dmitriev, L. Dubrovinsky, T. Le Bihan, A. Kuznetsov, H.-P. Weber, and E. G. Poniatovsky, Phys. Rev. B **73**, 094114 (2006).
[83] J.-C. Labiche, O. Mathon, S. Pascarelli, M. A. Newton, G. G. Ferre, C. Curfs, G. Vaughan, A. Homs, and D. F. Carreiras, Rev. Sci. Instrum. **78**, 091301 (2007).
[84] A. P. Hammersley, European Synchrotron Radiation Facility Internal Report No. ESRF98HA01T, 1998.
[85] D. T. Cromer, J. Chem. Phys. **50**, 4857 (1969).
[86] E. N. Maslen, A. G. Fox, and M. A. O'Keefe, in *International Tables for Crystallography* edited by A. J. C. Wilson (Kluwer, Dordrecht, 1995), Vol C, Sec. 6.1.1, p. 476.
[87] P. S. Salmon, S. Xin, and H. E. Fischer, Phys. Rev. B **58**, 6115 (1998).
[88] D. M. North, J. E. Enderby, and P. A. Egelstaff, J. Phys. C **1**, 784 (1968).
[89] J. L. Yarnell, M. J. Katz, R. G. Wenzel, and S. H. Koenig, Phys. Rev. A **7**, 2130 (1973).
[90] H. H. Paalman and C. J. Pings, J. Appl. Phys. **33**, 2635 (1962).
[91] A. K. Soper and P. A. Egelstaff, Nucl. Instrum. Methods **178**, 415 (1980).
[92] A. B. Bhatia and D. E. Thornton, Phys. Rev. B **2**, 3004 (1970).
[93] P. S. Salmon, Proc. R. Soc. London, Ser. A **445**, 351 (1994).
[94] E. Lorch, J. Phys. C **2**, 229 (1969).
[95] P. S. Salmon, J. Phys. F: Met. Phys. **18**, 2345 (1988).
[96] J. Neuefeind and K.-D. Liss, Ber. Bunsenges. Phys. Chem. **100**, 1341 (1996).
[97] D. L. Price, M.-L. Saboungi, and A. C. Barnes, Phys. Rev. Lett. **81**, 3207 (1998).
[98] R. Hussin, R. Dupree, and D. Holland, J. Non-Cryst. Solids **246**, 159 (1999).
[99] J. D. Jorgensen, J. Appl. Phys. **49**, 5473 (1978).
[100] B. Houser, N. Alberding, R. Ingalls, and E. D. Crozier, Phys. Rev. B **37**, 6513 (1988).
[101] J. A. E. Desa, A. C. Wright, and R. N. Sinclair, J. Non-Cryst. Solids **99**, 276 (1988).
[102] A. C. Hannon, D. Di Martino, L. F. Santos, and R. M. Almeida, J. Phys. Chem. B **111**, 3342 (2007).
[103] E. Fay, H. Völlenkle, and A. Wittmann, Z. Kristallogr. **138**, 439 (1973).
[104] B. Harbrecht, J. Kushauer, and H.-J. Weber, Eur. J. Solid State Inorg. Chem. **27**, 831 (1990).
[105] A. C. Hannon, D. Di Martino, L. F. Santos, and R. M. Almeida, J. Non-Cryst. Solids **353**, 1688 (2007).
[106] U. Hoppe, R. Kranold, H.-J. Weber, and A. C. Hannon, J. Non-Cryst. Solids **248**, 1 (1999).
[107] J. Haines, J. M. Léger, C. Chateau, and A. S. Pereira, Phys. Chem. Miner. **27**, 575 (2000).